Miner Petrol (2017) 111:853–863
DOI 10.1007/s00710-017-0494-2

ORIGINAL PAPER

Effect of dehydration on the electrical conductivity of phyllite at high temperatures and pressures

Wenqing Sun[1,2] · **Lidong Dai**[1] · **Heping Li**[1] · **Haiying Hu**[1,3] · **Jianjun Jiang**[1,2] · **Keshi Hui**[1,2]

Received: 7 July 2016 / Accepted: 17 January 2017 / Published online: 2 February 2017

Abstract The electrical conductivity of phyllite (measured in situ at 0.5–2.5 GPa and 773–1173 K) increases with increasing temperature, satisfying an Arrhenius relation. Dehydration of phyllite at 973–1173 K enormously enhances its electrical conductivity, and the activation enthalpy (0.64–0.81 eV) remains almost constant before and after dehydration. The inflection point of the relationship between electrical conductivity and temperature is used to determine the dehydration temperature (T_d) at each considered pressure (P), leading to the following relationship: $T_d = 1181 - 100P$. The derived relation implies that the dehydration depths of hot and cold subduction zones are ~70 and ~129 km respectively, which are both close to the depths of arc magma source regions, thereby indicating that the dehydration of pelite significantly influences the generation of melt in subduction zones.

Keywords High temperature and high pressure · Electrical conductivity · Phyllite · Dehydration · Subduction zone

Editorial handling: M.A.T.M. Broekmans

✉ Lidong Dai
dailidong_2014@hotmail.com

[1] Key Laboratory of High-Temperature and High-Pressure Study of the Earth's Interior, Institute of Geochemistry, Chinese Academy of Sciences, Guiyang 550081, China

[2] University of Chinese Academy of Sciences, Beijing 100049, China

[3] Key Laboratory of Earth and Planetary Physics, Institute of Geology and Geophysics, Chinese Academy of Sciences, Beijing 100029, China

Introduction

Understanding the material composition and thermodynamic state of the Earth's interior requires in situ measurements of the electrical conductivity of minerals and rocks at high temperatures and pressures, and comparison with magnetotelluric (MT) and geomagnetic depth sounding (GDS) results. Previous works have measured the electrical conductivities of many minerals and rocks in the crust and upper mantle, and suggested interpretations of high-conductivity layers (HCLs) in the Earth's interior (Zhu et al. 2001; Huang et al. 2005; Yang 2012; Cherevatova et al. 2014; Dai and Karato 2014a; Hu et al. 2014; Rao et al. 2014). However, little research has considered the electrical properties of pelite, a clastic rock in subduction zones, meaning that previous studies on the physical and chemical properties of subduction zones remain incomplete. Therefore, previous interpretations of HCLs should be reconsidered.

Pelites come in different forms (e.g., mudstone, clay rock, shale, and slate) and can transform to phyllite during metamorphism. Phyllite contains abundant sericite and chlorite, which are important hydrous minerals in subduction zones (Tatsumi and Eggins 1995; Cabral et al. 2012; Micheuz et al. 2015). As the subducting slab is heated and compressed, the pelites undergo a series of metamorphic changes (Wyllie 1982). Previous experimental petrological studies have shown that the dehydration of pelite at high temperatures and pressures accompanies the formation of new mineralogical phases (Tatsumi and Eggins 1995; Zhao et al. 2015). The dehydration temperature of minerals and rocks is generally determined using high-pressure differential thermal analysis and the inflection point of the Arrhenius relation between electrical conductivity and temperature (Song et al. 1996; Li et al. 2005). Previous works have demonstrated that dehydration can greatly enhance the electrical conductivity of minerals and rocks at

high temperatures and pressures (Song et al. 1996; Hicks and Secco 1997; Fuji-Ta et al. 2007a). Therefore, the dehydration temperature can be directly determined from the measurable increase of electrical conductivity. This temperature is a crucial parameter to determine the dehydration depth of pelite in a subduction zone.

This work reports the electrical conductivity of phyllite measured in situ at 0.5–2.5 GPa, 773–1173 K, and 10^{-1}–10^{6} Hz. At each pressure, the inflection point of the Arrhenius relation between electrical conductivity and temperature was used to determine the dehydration temperature of the phyllite, and the conduction mechanisms at different stages were explored in detail. Furthermore, a relationship between dehydration temperature and pressure was successfully established, and the dehydration depths of phyllite in hot and cold subduction zones were determined according to the dehydration conditions and the geothermal gradient in each case. Because the dehydration depth range of pelite is similar to that of arc magma source regions, we suggest that the dehydration of pelite significantly influences the generation of melt in subduction zones. The high electrical conductivity observed after dehydration can also account for the HCLs of certain regions in subduction zones.

Experimental procedures

Sample preparation

Fresh, brown phyllite samples were collected from the Fangshan District, Beijing, China. Their mineralogical composition was determined using optical microscopy and scanning electron microscopy (SEM) at the State Key Laboratory of Ore Deposit Geochemistry, Institute of Geochemistry, Chinese Academy of Sciences (CAS), Guiyang, China. By volume, the main minerals in the phyllite were chlorite (50%), sericite (30%), and quartz (14%), with minor albite (6%).

The phyllite samples were ultrasonically cleaned in a mixture of acetone and ethanol, and ground to powder (<200 mesh) in an agate mortar before being dried in a furnace at 473 K for 3 h. The powder was loaded into a copper capsule with a 0.025-mm thick Ni-foil liner, which prevented interdiffusion between the sample and the copper capsule during hot-press sintering. The height of the copper capsule was 18 mm, and its inner and outer diameters were 8.0 mm and 8.5 mm, respectively. To avoid the influence of pores and micro-cracks on the electrical conductivity results, the powdered samples were sintered for 3 h in a multi-anvil high-pressure apparatus at 2.0 GPa and 673 K, similar to the approach of Li et al. (2005). Then, the hydrothermally annealed samples were cut and polished into cylinders with diameter and height of 6 mm. Finally, the samples were baked at 473 K for 8 h to eliminate any absorbed water that might have affected the electrical conductivity measurements.

Impedance measurements

Measurements were carried out using a YJ-3000 t multi-anvil press and a Solartron-1260 Impedance/Gain-phase analyzer at the Key Laboratory of High-Temperature and High-Pressure Study of the Earth's Interior, Institute of Geochemistry, Chinese Academy of Sciences (CAS), Guiyang, China. Details of the measurement procedures are given by Dai et al. (2009) and Hu et al. (2013). The multi-anvil press can achieve pressures of up to 6.0 GPa, and six cubic WC anvils were assembled and compressed. Temperatures of up to 2273 K can be achieved with a lanthanum chromate heater, but the temperature range considered here was attained using a stainless steel heater (~298–1573 K). Errors in the electrical conductivity measurements were estimated to be less than 5%, and the principal sources of error were dimensional changes in the sample (<8%), experimental temperature error (<10 K), and experimental pressure error (<0.1 GPa).

The experimental assemblage for the electrical conductivity measurements is shown in Fig. 1. Pyrophyllite cubes of 32.5 mm edge length were used as the pressure medium, and three-layer stainless steel sheets (total thickness 0.5 mm) arranged around the Al_2O_3 insulator were applied as the heater. To shield against external electromagnetic and spurious signal interference, a layer of Ni foil (thickness 0.025 mm) was installed between the Al_2O_3 insulation and the MgO sleeve. The sample was loaded into the MgO tube, and two Ni disks (diameter 6 mm, thickness 0.5 mm) on the top and bottom of sample comprised the parallel-plate electrode. To prevent free water from influencing the impedance spectra measurements, all components of the apparatus (pyrophyllite, ceramic tubes, Al_2O_3, and MgO sleeves) were heated at 1073 K for 8 h in a muffle furnace. Temperatures were measured with a NiCr-NiAl thermocouple, and the pressure and temperature errors were ±0.1 GPa and ±10 K, respectively.

During the experiments, pressure was slowly increased at a rate of 1.0 GPa/h to the desired value, then temperature increased at 100 K/h to the designated values. Once the temperature reached a stable value, the impedance spectra were measured with an applied voltage of 1 V using a frequency range of 10^{-1} to 10^{6} Hz. Moisture can potentially influence the validity and precision of electrical conductivity measurements for minerals and rocks at high temperatures and pressures (Manthilake et al. 2009; Shatskiy et al. 2009; Yoshino et al. 2010; Dai et al. 2015; Hu et al. 2015), and its effects were mitigated here by maintaining the experimental assembly for at least 3 h at high temperature (773 K) and high pressure (0.5, 1.5, and 2.5 GPa) during the impedance spectroscopy measurements. When two successive impedance spectra were almost completely overlapping, we started to collect each data

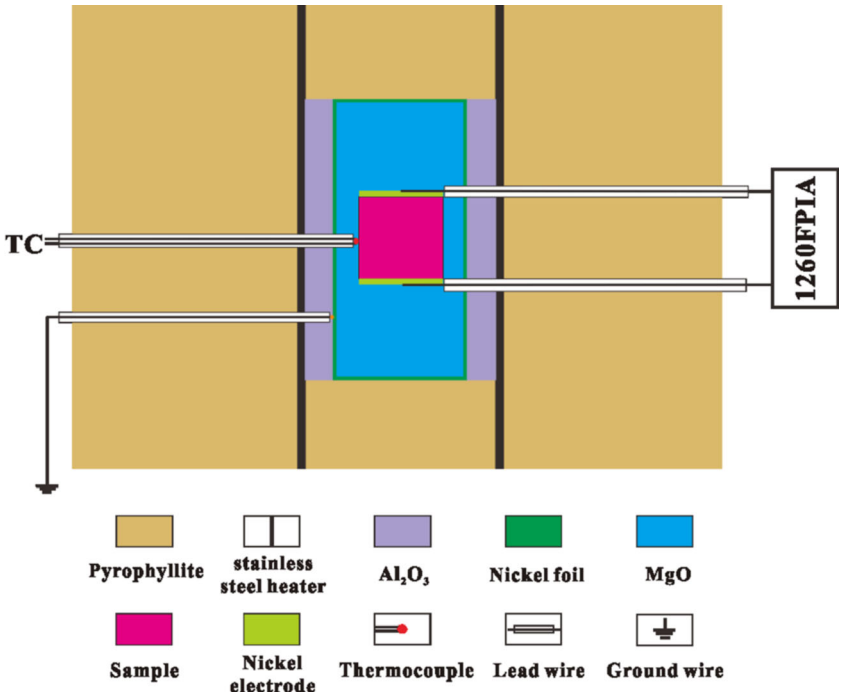

Fig. 1 Experimental setup of electrical conductivity measurements

point at intervals of 50 K. This ensured that all the conductivity results were obtained at a steady state condition. Furthermore, two heating and cooling cycles were conducted to confirm further the elimination of any moisture effect during the measurements. Two representative heating and cooling cycles at 1.5 GPa are displayed in Fig. 2. Overall, the influence of moisture on the electrical conductivity of phyllite was negligible. Impedance spectra of the phyllite samples were collected at 0.5–2.5 GPa and 773–1173 K.

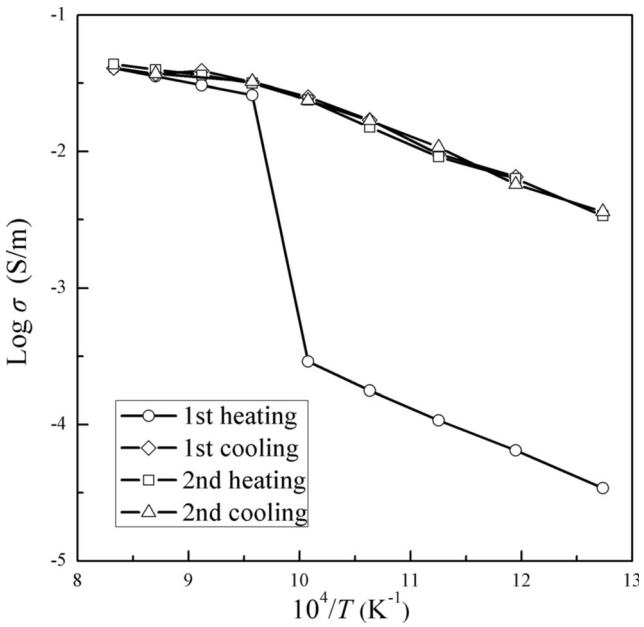

Fig. 2 Logarithm of electrical conductivity versus reciprocal temperature for the sample during different heating/cooling cycles at 1.5 GPa

Results

Typical Nyquist and Bode diagrams measured at 1.5 GPa and 773–1173 K are shown in Figs. 3 and 4, respectively. The real part (Z'), imaginary part (Z''), modulus ($|Z|$), and phase angle (θ) of the impedance spectra follow the relationships $Z' = |Z|\cos\theta$ and $Z'' = |Z|\sin\theta$ (Nover et al. 1992; Huebner and Dillenburg 1995). The impedance spectra in Fig. 3 each include an integrated semicircle and a straight line at 773–973 K, but only show a complete semicircle at 1023–1173 K. Generally, the semicircle occurring at high frequency represents the impedance of the grain interior, and the tail at low frequency represents the impedance of the grain boundary or the sample-electrode interface. Furthermore, the complete arc representing grain-boundary conduction occurs at the intermediate frequency range of 0.01–200 Hz (Roberts and Tyburczy 1991), whereas the electrode response can appear separately or as a straight line, which is characteristic of diffusion at the sample-electrode interface (MacDonald 1992; Hu et al. 2015). Therefore, the additional linear section observed here reflects the effect of the electrodes, and the bulk sample resistance can be determined by fitting the first semicircular arc. The equivalent circuit shown in Fig. 3 has resistor (R) and constant-phase element (CPE) components for the bulk impedance for the sample (R_s and CPE_s, respectively) and for the sample-electrode interface (R_E and CPE_E, respectively).

The fitting error is less than 5%. The electrical conductivity of the sample was calculated as follows:

$$\sigma = L/SR, \tag{1}$$

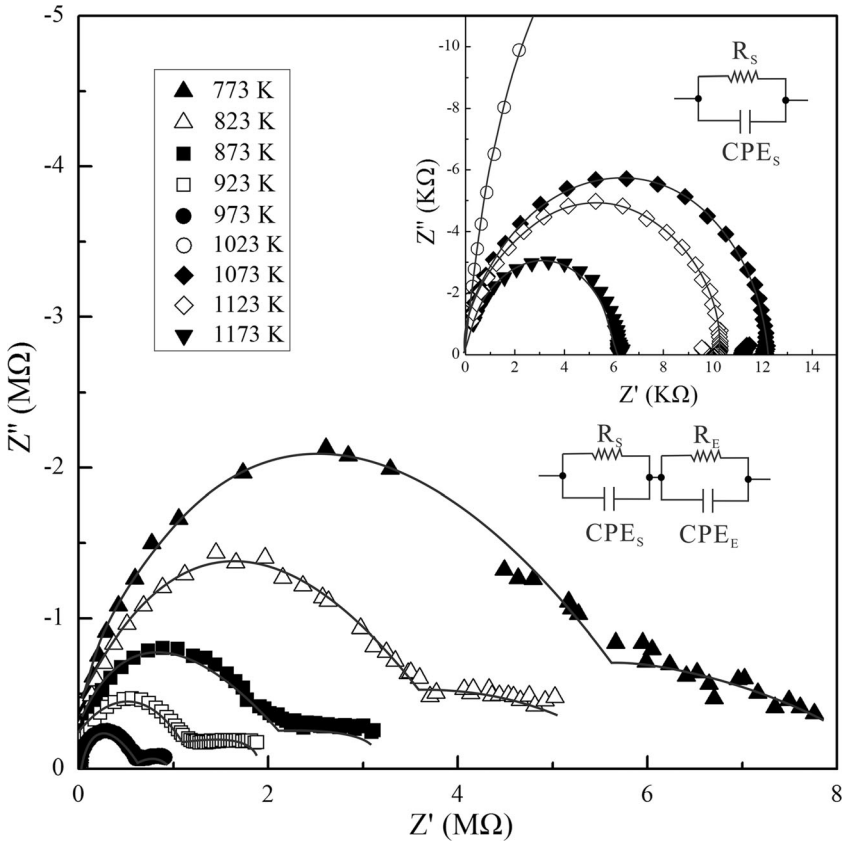

Fig. 3 Nyquist plot of the complex impedance of phyllite at 1.5 GPa and 773–1173 K

where L is the height of the sample (m), S is the cross-sectional area of the electrodes (m^2), R is the fitting resistance (Ω), and σ is the electrical conductivity of the sample (S/m).

The logarithmic electrical conductivity of phyllite is plotted against the reciprocal temperature in Fig. 5 for pressures of 0.5–2.5 GPa and temperatures of 773–1173 K. The

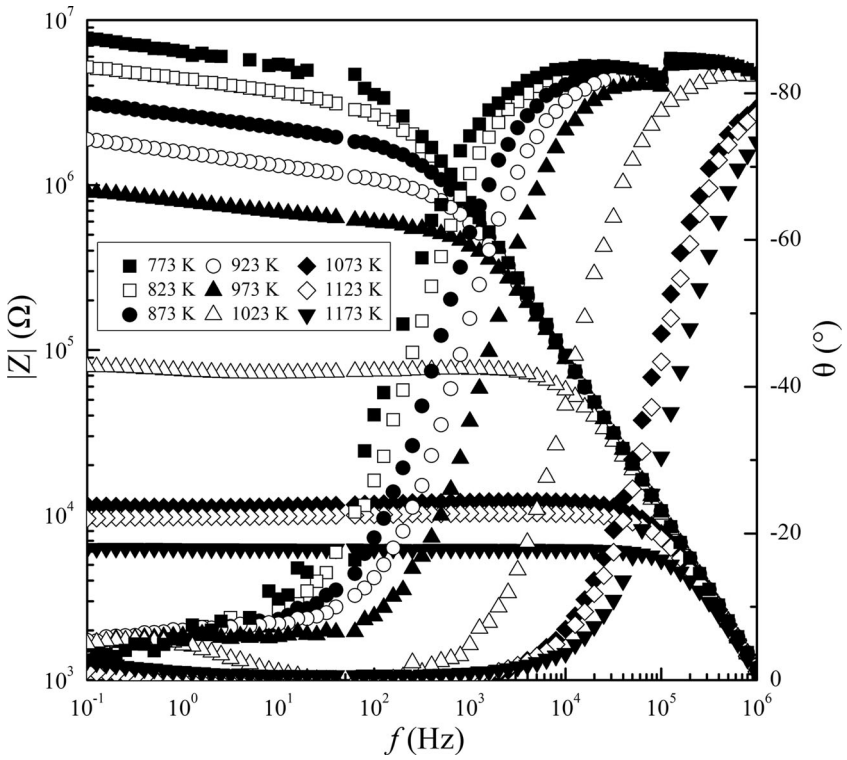

Fig. 4 Bode plot of phyllite at 1.5 GPa and 773–1173 K

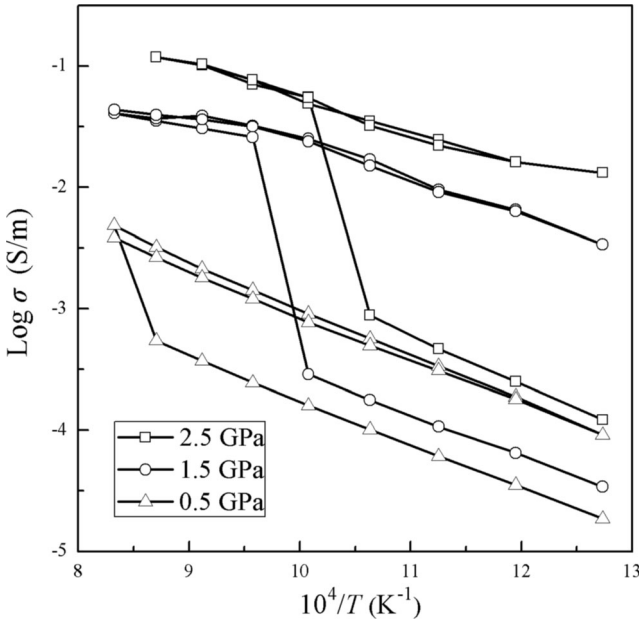

Fig. 5 Relationship between electrical conductivity of phyllite and reciprocal temperature at 0.5–2.5 GPa and 773–1173 K

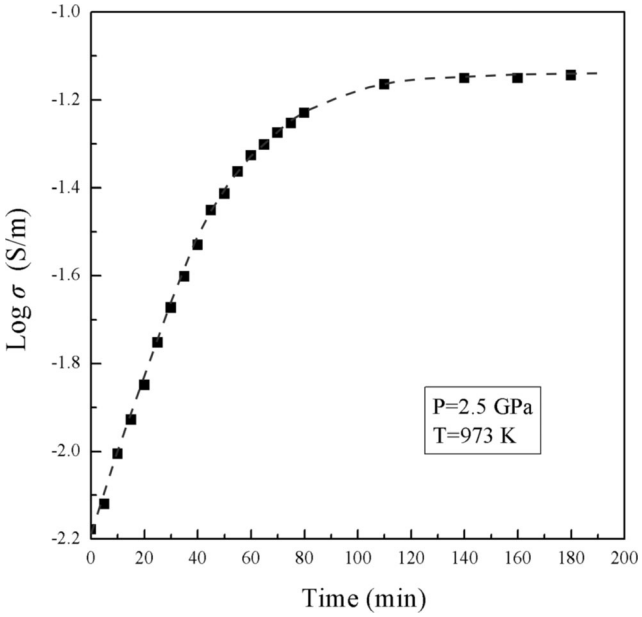

Fig. 6 Relationship between electrical conductivity of phyllite and time at 2.5 GPa and 973 K

relationship between electrical conductivity and temperature before dehydration fits the Arrhenius formula:

$$\sigma = \sigma_0 \exp(-\Delta H/kT) \quad (2)$$

where σ_0 is a pre-exponential factor (K·S/m), ΔH is the activation enthalpy (eV), k is the Boltzmann constant (eV/K), and T is absolute temperature (K). The fitting parameters for the bulk sample conductivity are listed in Table 1.

The progression in electrical conductivity with time during dehydration is shown in Fig. 6 for a sample held at 2.5 GPa and 973 K. The electrical conductivity increases sharply in the initial 40 min and then gradually levels off, reaching a steady state after 180 min. The attainment of constant electrical conductivity indicates the completion of dehydration. The mineral associations of the phyllite sample before and after dehydration were accurately determined, and the results of optical microscopy and SEM are shown in Figs. 7 and 8 and listed in Table 2. At 0.5 GPa, the dehydration temperature of the sample was 1173 K, and partial melting occurred during dehydration. After dehydration, the electrical conductivity showed good repeatability during cooling and heating. At 1.5 and 2.5 GPa, the dehydration temperatures were 1023 and 973 K, respectively. New minerals (garnet, biotite, and kyanite) appeared in the experimental products during dehydration, and no melt appeared (Figs. 7 and 8). The electrical conductivity slowly increased upon heating after dehydration, and showed good repeatability during cooling and heating. While the electrical conductivity of the sample increased with increasing pressure, the effect was relatively weak before dehydration. However, the electrical conductivity of the sample at 0.5 GPa was more than two orders of magnitude lower than that at 1.5 or 2.5 GPa after dehydration.

Table 1 Fitted parameters for the electrical conductivity of phyllite before dehydration

Run no.	P (GPa)	T (K)	Log σ_0 (S/m)	ΔH (eV)	R^2
DS2	0.5	773–1073	-0.21 ± 0.01	0.69 ± 0.01	0.9969
DS3	1.5	773–973	-0.10 ± 0.01	0.64 ± 0.01	0.9991
DS4	2.5	773–923	1.35 ± 0.04	0.81 ± 0.01	0.9989

Discussion

Comparison with published data

The volumetrically abundant chlorite and sericite appear to dominate the electrical conductivity of the phyllite samples. Conductivities were ~10^{-3} S/m before dehydration. At 0.5 GPa, partial melting occurred during dehydration, with the melt occupying a volume fraction of about 0.5%. At 1.5 and 2.5 GPa, new minerals (garnet, biotite, and kyanite) appeared with no melt. Partial melting generally enhances the electrical conductivity of silicate minerals and rocks (e.g., Schilling et al. 1997; Maumus et al. 2005), but here the electrical conductivity of phyllite after partial melting at 0.5 GPa was 2–2.5 orders of magnitude lower than that with no melt at 1.5 or 2.5 GPa. This result might reflect the occurrence of abundant biotite (20%) in the dehydration products at higher pressures. Li et al. (2016) confirmed that the electrical conductivity of phlogopite is much higher than that of peridotite, serpentine,

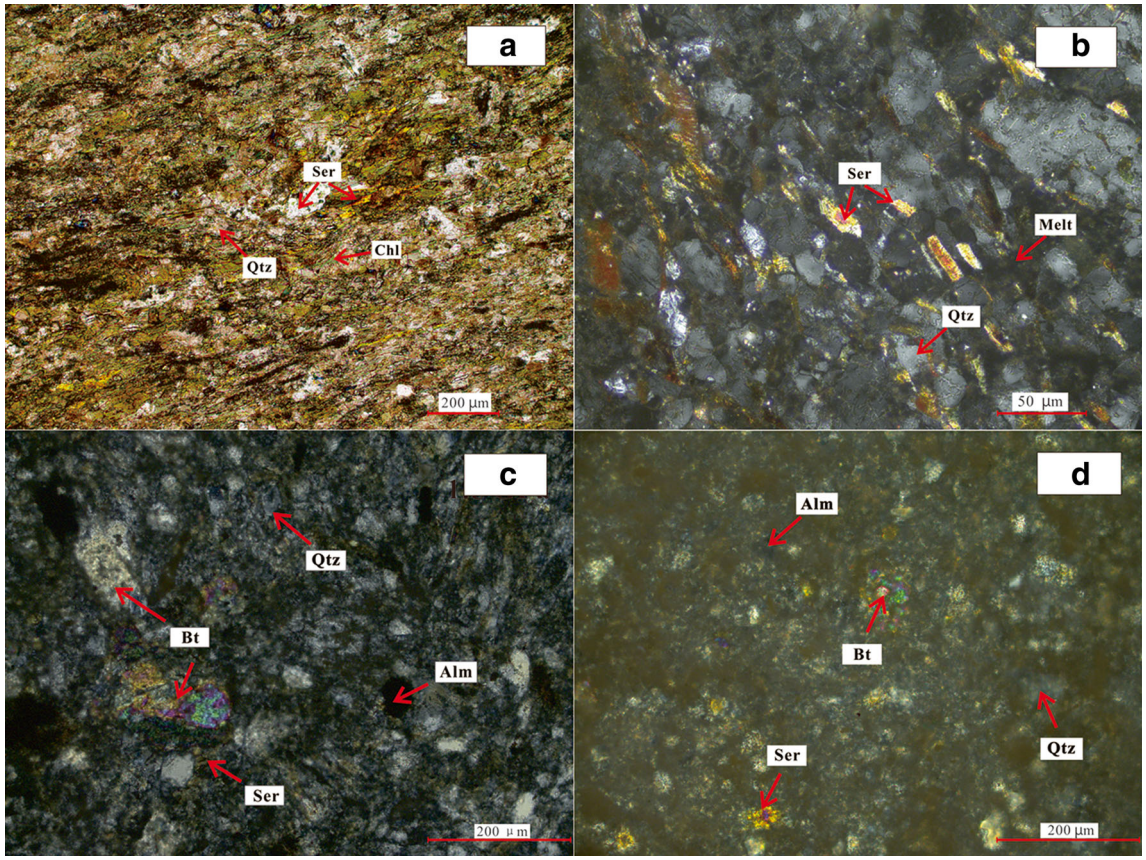

Fig. 7 Photomicrographs of (**a**) the original phyllite sample and the experimental products at (**b**) 0.5 GPa, (**c**) 1.5 GPa, and (**d**) 2.5 GPa. Qtz = quartz, Chl = chlorite, Ser = sericite, Bt = biotite, Alm = almandine, Ky = kyanite, Ab = albite

talc, or pyrophyllite; therefore, a small quantity of phlogopite can significantly enhance the electrical conductivity of silicate rocks. Given that biotite and phlogopite belong to the same group of mica minerals, having similar crystal textures and

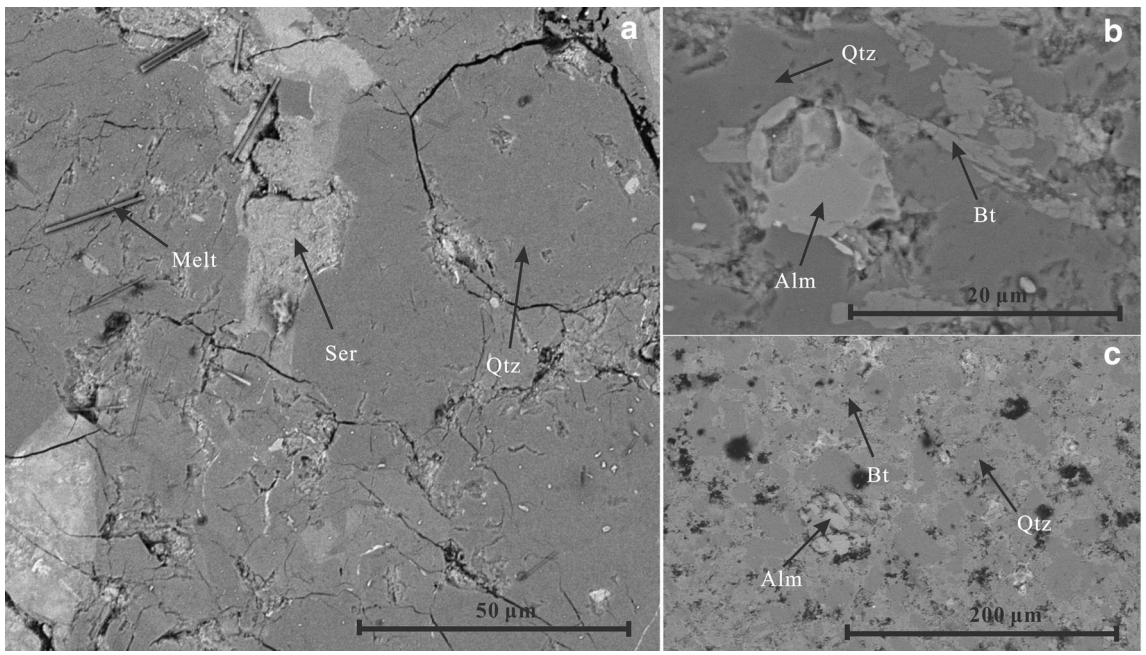

Fig. 8 Electron backscattered images of the recovered samples after EC measurements at (**a**) 0.5 GPa, (**b**) 1.5 GPa, and (**c**) 2.5 GPa. Qtz = quartz, Ser = sericite, Bt = biotite, Alm = almandine

Table 2 Mineralogical assemblage of original sample and experimental products

	P (GPa)	*T* (K)	No.	Mineral associations
Before dehydration	/	/	DS1	Chl (50%) + Ser (30%) + Qtz (14%) + Ab (6%)
	0.5	773–1173	DS2	Qtz (70%) + Ser (25%) + Ab (4.5%) + Melt (0.5%)
After dehydration	1.5	773–1173	DS3	Qtz (40%) + Alm (20%) + Bt (20%) + Ser (10%) + Ab (6%) + Ky (4%)
	2.5	773–1123	DS4	Qtz (40%) + Alm (20%) + Bt (20%) + Ser (10%) + Ab (6%) + Ky (4%)

chemical components, their electrical conductivities might be similar. The biotite observed here might therefore have a more significant effect on the electrical conductivity of the sample than the partial melting observed at lower pressure. The abundant biotite (20%) in the dehydration products show good interconnectivity (Fig. 8). Comparison with the results of Manthilake et al. (2015) shows that aqueous fluid is less conductive than the dehydration products of phyllite. The interconnected biotites were thus possibly responsible for the high electrical conductivity of the dehydration products of phyllite at 1.5 and 2.5 GPa. On the other hand, SEM analyses revealed dehydration-induced partial melting in the phyllite at 0.5 GPa, which can reasonably explain the about one order of magnitude enhancement of electrical conductivity seen at 1173 K. However, the volume fraction of melt was relatively low, only ~0.5%, and therefore the electrical conductivity of phyllite at 0.5 GPa was lower than that at 1.5 or 2.5 GPa. The presence of sericite in the dehydration products made the partial dehydration of phyllite obvious. We also estimated the mass fraction of fluid released to the sample during dehydration at each of the three tested pressures to be ~4.0 wt%.

The maximum electrical conductivity of chlorite is 10^{-4} S/m before dehydration (Manthilake et al. 2016), slightly lower than that of the phyllite considered here. This discrepancy might be due to the influence of sericite in the phyllite. Similar to other silicate minerals and rocks, the electrical conductivity of phyllite shows a weak pressure dependence (Dai et al. 2008, 2012, 2013, 2014, 2015; Yang and McCammon 2012; Manthilake et al. 2016), increasing slightly under compression before dehydration, like chlorite (Manthilake et al. 2016). After dehydration, the electrical conductivity of phyllite increases by two orders of magnitude, thereby confirming the significant influence of the dehydration of hydrous minerals and rocks (Zhu et al. 1999; Fuji-ta et al. 2007a; Manthilake et al. 2016). Although the dehydration temperature of chlorite is similar to that of phyllite, the dehydrated mineral assemblages of chlorite and phyllite are different. Our phyllite was dominated by garnet, biotite, and kyanite after dehydration (Table 2); however, the hydrous chlorite reported by Manthilake et al. (2016) comprised mainly magnetite, olivine, and pyrope after dehydration.

Phyllite is a representative low-grade metamorphic rock in regional metamorphic belts, and its metamorphic grade increases with increasing pressure and temperature to become gneiss and granulite. Comprehensive research into the electrical properties of regional metamorphic belts would require the electrical conductivities of all three of these metamorphic rocks to be compared. Fuji-ta et al. (2007b) studied gneiss in the Higo metamorphic zone in Japan and found that its electrical conductivity in the direction parallel to the foliation is 0.5–1.5 orders of magnitude higher than that perpendicular to the foliation. Fuji-ta et al. (2004) studied the electrical conductivity of granulite that formed in the lower crust, in the zone of metamorphism, and reported that its electrical conductivities at high and low temperatures were similar to those reported by Satoh et al. (1998) and Ogawa et al. (1994), respectively. Compared with gneiss and granulite, the electrical conductivity of phyllite after dehydration at 1.5 GPa is similar to that of granulite and slightly lower than that of gneiss. These differences might arise from the samples' different mineral compositions and rock textures. Serpentinite is an important rock in subduction zones, and previous studies have indicated that its dehydration might account for the HCLs in such settings (Robertson et al. 2015). Phyllite is less electrically conductive than serpentinite both before and after dehydration, and the dehydration temperature of serpentinite is 100 K lower than that of phyllite at a given pressure (Zhu et al. 1999; Xie et al. 2002). The dehydration products of phyllite, gneiss, and granulite show similar slopes on a log σ versus $1/T$ diagram, which might indicate that the three metamorphic rocks have the same conduction mechanism (Fig. 9).

Conduction mechanism

The electrical conductivity of the phyllite samples before dehydration follows an Arrhenius relation with respect to temperature, indicating the presence of only one conduction mechanism. Fitting to the Arrhenius relation gives an activation enthalpy range of 0.69–0.81 eV (Table 1). The slope of the straight line after dehydration is similar to that before dehydration (Fig. 5).

Small polarons are considered to be the main charge carriers in Fe-bearing dry, nominally anhydrous minerals (e.g., Dai and Karato 2009a, b; Yang et al. 2012; Yang and McCammon 2012; Dai et al. 2016) and in some Fe-bearing nominally hydrous silicate minerals and rocks such as

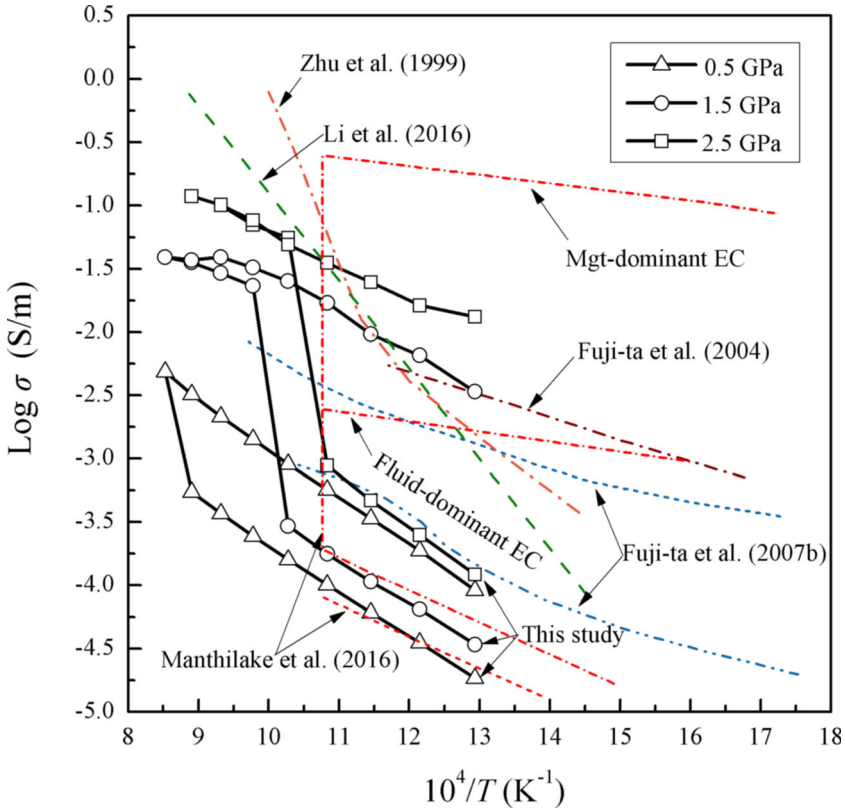

Fig. 9 Comparison of the electrical conductivity of phyllite measured in this study and previous studies

chlorite, pyrophyllite, and serpentinite (Zhu et al. 1999, 2001; Reynard et al. 2011; Manthilake et al. 2016). Chlorite is the main mineral component of the phyllite samples, and its conduction mechanism dominates the conduction in the bulk rock. The activation enthalpy range for chlorite before dehydration is 0.55–0.56 eV, and small polaron conduction is proposed to be the dominant conduction mechanism in the chlorite at high pressures and temperatures (Manthilake et al. 2016). The activation enthalpy for chlorite is slightly lower than that for the phyllite samples, which might be linked to the phyllite's complex crystallographic structure and mineralogical composition. In addition, the calculated activation enthalpies for phyllite before and after dehydration are similar (Fig. 5). Therefore, small polaron conduction is suggested to be the dominant conduction mechanism, with the following conduction process:

$$Fe^{\times}_{Mg} + h^{\cdot} \rightleftarrows Fe^{\cdot}_{Mg}, \quad (3)$$

Where $Fe^{\times}_{Mg}$ and $Fe^{\cdot}_{Mg}$ are divalent and trivalent Fe ions at Mg lattice sites, respectively, and $h^{\cdot}$ is an electron hole, which migrates along the same direction as the small polaron ($Fe^{\cdot}_{Mg}$) in an electrical field.

Geophysical implications

The various constituent minerals examined here, before and after dehydration, are consistent with the two main metamorphic reactions that occur in subduction zones (Tatsumi and Eggins 1995):

$$2(Mg,Fe)_{4.5}\,Al_3Si_{2.5}O_{10}(OH)_8 + 4SiO_2 = 3(Mg,Fe)_3\,Al_2Si_3O_{12} + 8H_2O, \quad (4)$$

$$3(Mg,Fe)_5\,Al_2Si_3O_{10}(OH)_8 + 5KAI_3Si_3O_{10}(OH,F)_2 = 8Al_2SiO_5 + 5K(Mg,Fe)_3\,AlSi_3O_{10}(OH,F)_2 + SiO_2 + 12H_2O \quad (5)$$

Therefore, the dehydration depth of pelite in a subduction zone can be determined based on the geothermal gradient and the relationship between dehydration temperature and pressure.

The observed inflection points in the relationship between electrical conductivity and temperature indicate the dehydration temperatures at 0.5, 1.5, and 2.5 GPa to be 1173, 1023, and 973 K, respectively. The dehydration temperature (T_d) of the phyllite observed here shows a linear relationship with pressure (P): $T_d = 1181 - 100P$. Li et al. (2005) studied the pressure dependence of the dehydration temperature of pelite, finding a relationship of $T = 1165–70.6P$ using high-pressure differential thermal analysis (HP-DTA). Although the mineral species of the two rocks are similar, they have different proportions of hydrous minerals; their different dehydration temperatures might also be caused by different measurement methods.

As shown in Fig. 10, the geothermal gradients at cold and hot subduction zones are 4 and 10 K/km, respectively (Ahrens 1989; Peacock 1990). The corresponding dehydration points for phyllite are 3.8 GPa and 801 K and 2.0 GPa and 981 K, respectively, which occur at depths of 129 and 70 km, respectively. Previous studies have confirmed a depth range of 90–150 km as the source of arc magma (Tatsumi 1989; Saunders et al. 1991; Spandler and Pirard 2013; Bebout and Penniston-Dorland 2016). Hence, we suggest that the dehydration of pelite contributes to the development of magma in subduction zones.

Previous studies have confirmed that HCLs can be caused by hydrogen in nominally anhydrous minerals, aqueous fluid, silicate melt, carbonate melt, and graphite layers (Duba and Shankland 1982; Hyndman et al. 1993; Maumus et al. 2005; Gaillard et al. 2008; Yang et al. 2011; Dai and Karato 2014a, b, c, d; Manthilake et al. 2015). This study provides further evidence to suggest that biotite in the dehydration products of phyllite can cause HCLs. HCLs in subduction zones are generally thought to be caused by the dehydration of serpentinite (Robertson et al. 2015; Zhang et al. 2015), and the influence of pelite is disregarded. The electrical conductivity of phyllite after dehydration was observed here to be 10^{-2} to 10^{-1} S/m, a range of values similar to those of the HCLs of the middle and lower crust in subduction zones (Robertson et al. 2015). Therefore, the dehydration product of pelite might be the cause of the HCLs in subduction zones, where pelite is potentially abundant and widespread.

Conclusions

Based on the newly acquired data as elaborated and discussed above, the following conclusions can be drawn:

1) The electrical conductivity of phyllite significantly increases with increasing temperature, and slightly increases with increasing pressure.
2) The dehydration temperature of phyllite ranges from 973 to 1173 K at 0.5–2.5 GPa, and dehydration dramatically enhances its electrical conductivity.
3) Interconnected biotite is proposed to be responsible for the high electrical conductivity of the dehydration products of phyllite at 1.5 and 2.5 GPa. Dehydration-induced partial melting is observed at 0.5 GPa; however, its limited volume fraction (~0.5%) does not raise the electrical conductivity of phyllite at 0.5 GPa above that at 1.5 or 2.5 GPa.
4) Given the calculated activation enthalpy and the results of previous studies, small polaron conduction is suggested to be the conduction mechanism of phyllite at high temperatures and pressures.
5) The dehydration depths of phyllite are similar to the depths of magmatic source regions; consequently, we infer that the dehydration of pelite contributes to the generation of magma in subduction zones.

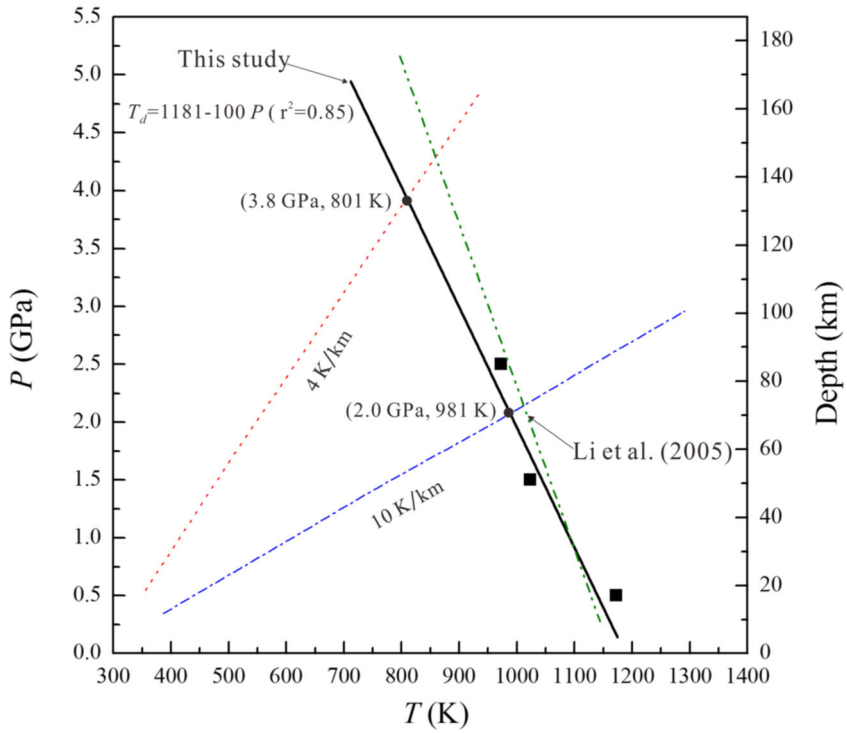

Fig. 10 Dehydration depths of pelite in hot and cold subduction zones

Acknowledgements Constructive reviews of two anonymous experts are gratefully acknowledged. This research was financially supported by the Strategic Priority Research Program (B) of the Chinese Academy of Sciences (XDB 18010401), Key Research Projects of the Frontier Science of the Chinese Academy of Sciences (QYZDB-SSW-DQC009), "135" Program of the Institute of Geochemistry of CAS, Hundred Talents Program of CAS, Youth Innovation Promotion Association of CAS, NSF of China (41474078, 41304068 and 41174079) and Open Foundation of Institute of Geology and Geophysics of CAS.

References

Ahrens TJ (1989) Water storage in the mantle. Nature 342:122–123

Bebout GE, Penniston-Dorland SC (2016) Fluid and mass transfer at subduction interfaces − The field metamorphic record. Lithos 240-243:228–258

Cabral AR, Wiedenbeck M, Koglin N, Lehmann B, Abreu FRD (2012) Boron-isotopic constraints on the petrogenesis of hematitic phyllite in the southern Serra do Espinhaco, Minas Gerais, Brazil. Lithos 140:224–233

Cherevatova M, Smirnov M, Korja T, Kaikkonen P, Pedersen LB, Hübert J, Kamm J, Kalscheuer T (2014) Crustal structure beneath southern Norway imaged by magnetotellurics. Tectonophysics 628:55–70

Dai LD, Karato SI (2009a) Electrical conductivity of wadsleyite at high temperatures and high pressures. Earth Planet Sci Lett 287:277–283

Dai LD, Karato SI (2009b) Electrical conductivity of pyrope-rich garnet at high temperature and high pressure. Phys Earth Planet Inter 176: 83–88

Dai LD, Karato SI (2014a) High and highly anisotropic electrical conductivity of the asthenosphere due to hydrogen diffusion in olivine. Earth Planet Sci Lett 408:79–86

Dai LD, Karato SI (2014b) The effect of pressure on the electrical conductivity of olivine under the hydrogen-rich conditions. Phys Earth Planet Inter 232:51–56

Dai LD, Karato SI (2014c) Influence of oxygen fugacity on the electrical conductivity of hydrous olivine: implications for the mechanism of conduction. Phys Earth Planet Inter 232:57–60

Dai LD, Karato SI (2014d) Influence of FeO and H on the electrical conductivity of olivine. Phys Earth Planet Inter 237:73–79

Dai LD, Li HP, Hu HY, Shan SM (2008) Experimental study of grain boundary electrical conductivities of dry synthetic peridotite under high-temperature, high-pressure, and different oxygen fugacity conditions. J Geophys Res 113:B12211

Dai LD, Li HP, Hu HY, Shan SM (2009) Novel technique to control oxygen fugacity during high-pressure measurements of grain boundary conductivities of rocks. Rev Sci Instrum 80:033903

Dai LD, Li HP, Hu HY, Shan SM, Jiang JJ, Hui KS (2012) The effect of chemical composition and oxygen fugacity on the electrical conductivity of dry and hydrous garnet at high temperatures and pressures. Contrib Mineral Petrol 163:689–700

Dai LD, Li HP, Hu HY, Jiang JJ, Hui KS, Shan SM (2013) Electrical conductivity of $Alm_{82}Py_{15}Grs_3$ almandine-rich garnet determined by impedance spectroscopy at high temperatures and high pressures. Tectonophysics 608:1086–1093

Dai LD, Hu HY, Li HP, Jiang JJ, Hui KS (2014) Influence of temperature, pressure, and chemical composition on the electrical conductivity of granite. Am Mineral 99:1420–1428

Dai LD, Hu HY, Li HP, Hui KS, Jiang JJ, Li J, Sun WQ (2015) Electrical conductivity of gabbro: the effects of temperature, pressure and oxygen fugacity. Eur J Mineral 27:215–224

Dai LD, Hu HY, Li HP, Wu L, Hui KS, Jiang JJ, Sun WQ (2016) Influence of temperature, pressure, and oxygen fugacity on the electrical conductivity of dry eclogite, and geophysical implications. Geochem Geophys Geosyst 17:2394–2407

Duba AG, Shankland TJ (1982) Free carbon and electrical conductivity in the Earth's mantle. Geophys Res Lett 9:1271–1274

Fuji-ta K, Katsura T, Tainosho Y (2004) Electrical conductivity measurement of granulite under mid- to lower crustal pressure-temperature conditions. Geophys J Int 157:79–86

Fuji-ta K, Katsura T, Matsuzaki T, Ichiki M (2007a) Electrical conductivity measurements of brucite under crustal pressure and temperature conditions. Earth Planets Space 59:645–648

Fuji-ta K, Katsura T, Matsuzaki T, Ichiki M, Kobayashi T (2007b) Electrical conductivity measurement of gneiss under mid- to lower crustal *P-T* conditions. Tectonophysics 434:93–101

Gaillard F, Malki M, Iacono-Marziano G, Pichavant M, Scaillet B (2008) Carbonatite melts and electrical conductivity in the asthenosphere. Science 322:1363–1365

Hicks TL, Secco RA (1997) Dehydration and decomposition of pyrophyllite at high pressures: electrical conductivity and X-ray diffraction studies to 5 GPa. Can J Earth Sci 34:875–882

Hu HY, Li HP, Dai LD, Shan SM, Zhu CM (2013) Electrical conductivity of alkali feldspar solid solutions at high temperatures and high pressures. Phys Chem Miner 40:51–62

Hu HY, Dai LD, Li HP, Jiang JJ, Hui KS (2014) Electrical conductivity of K-feldspar at high temperature and high pressure. Mineral Petrol 108:609–618

Hu HY, Dai LD, Li HP, Jiang JJ, Hui KS, Li J (2015) Temperature and pressure dependence of electrical conductivity in synthetic anorthite. Solid State Ionics 276:136–141

Huang XG, Xu YS, Karato S (2005) Water content in the transition zone from electrical conductivity of wadsleyite and ringwoodite. Nature 434:746–749

Huebner JS, Dillenburg RG (1995) Impedance spectra of hot, dry silicate minerals and rock-qualitative interpretation of spectra. Am Mineral 80:46–64

Hyndman RD, Vanyan LL, Marquis G (1993) The origin of electrically conductive lower continental crust: saline water or graphite? Phys Earth Planet Inter 81:325–344

Li Y, Tang HF, Liu CQ, Hou GS (2005) The high pressure differential thermal study of dehydration effect of pelite. Acta Petrol Sin 21: 986–992 (in Chinese)

Li Y, Yang XZ, Yu JH, Cai YF (2016) Unusually high electrical conductivity of phlogopite: the possible role of fluorine and geophysical implications. Contrib Mineral Petrol 171:1–11

Macdonald JR (1992) Impedance spectroscopy. Ann Biomed Eng 20: 289–305

Manthilake M, Matsuzaki T, Yoshino T, Yamashita S, Ito E, Katsura T (2009) Electrical conductivity of wadsleyite as a function of temperature and water content. Phys Earth Planet Inter 174:10–18

Manthilake G, Mookherjee M, Bolfan-Casanova N (2015) Electrical conductivity of lawsonite and dehydrating fluids at high pressures and temperatures. Geophys Res Lett 42:7398–7405

Manthilake G, Bolfan-Casanova N, Novella D, Mookherjee M, Andrault D (2016) Dehydration of chlorite explains anomalously high electrical conductivity in the mantle wedges. Sci Adv 2:e1501631

Maumus J, Bagdassarov N, Schmeling H (2005) Electrical conductivity and partial melting of mafic rocks under pressure. Geochim Cosmochim Acta 69:4703–4718

Micheuz P, Krenn K, Fritz H, Kurz W (2015) Tectonometamorphic evolution of blueschist-facies rocks in the phyllite-quartzite unit of the external hellenides (Mani, Greece). Austrian J Earth Sci 108:109–122

Nover G, Will G, Waitz R (1992) Pressure-induced phase-transition in Mg_2GeO_4 as determined by frequency-dependent complex electrical-resistivity measurements. Phys Chem Miner 19:133–139

Ogawa Y, Nishida Y, Makino M (1994) A collision boundary imaged by magnetotellurics, Hidaka mountains, Central Hokkaido, Japan. J Geophys Res 99:22373–22388

Peacock SM (1990) Numerical simulation of metamorphic pressure- temperature- time paths and fluid production in subducting slabs. Tectonics 9:1197–1211

Rao CK, Selvaraj C, Gokarn SG (2014) Deep electrical structure over the igneous arc of the indo Burman Orogen in Sagaing province, Myanmar from magnetotelluric studies. J Asian Earth Sci 94:68–76

Reynard B, Mibe K, Van de Moortele B (2011) Electrical conductivity of the serpentinised mantle and fluid flow in subduction zones. Earth Planet Sci Lett 307:387–394

Roberts JJ, Tyburczy JA (1991) Frequency dependent electrical properties of polycrystalline olivine compacts. J Geophys Res 96:16205–16222

Robertson K, Taylor D, Thiel S, Heinson G (2015) Magnetotelluric evidence for serpentinisation in a Cambrian subduction zone beneath the Delamerian Orogen, Southeast Australia. Gondwana Res 28: 201–211

Satoh H, Nishida Y, Utsugi M, Hirano K, Doi T, Arita K (1998) Resistivity structure in and around the southern part of Hidaka Metamorphic Belt, Hokkaido, as inferred from magnetotelluric investigations. Geophys Bull Hokkaido Univ 61:59–68 (in Japanese)

Saunders AD, Norry MJ, Tarney J (1991) Fluid influence on the trace element compositions of subduction zone magmas. Philos T Roy Soc A 335:377–392

Schilling FR, Partzsch GM, Brasse H, Schwarz G (1997) Partial melting below the magmatic arc in the Central Andes deduced from geoelectromagnetic field experiments and laboratory data. Phys Earth Planet Inter 103:17–31

Shatskiy A, Litasov K, Matsuzaki T, Shinoda K, Yamazaki D, Yoneda A, Ito E, Katsura T (2009) Single crystal growth of wadsleyite. Am Mineral 94:1130–1136

Song MS, Xie HS, Zheng HF, Guo J, Xu YS, Xu ZM (1996) Determination of serpentine dehydration temperature at 1–5 GPa by the method of electrical conductivity. Chin Sci Bull 41:1815–1819

Spandler C, Pirard C (2013) Element recycling from subducting slabs to arc crust: a review. Lithos 170-171:208–223

Tatsumi Y (1989) Migration of fluid phases and genesis of basalt magmas in subduction zones. J Geophys Res 94:4697–4707

Tatsumi Y, Eggins S (1995) Subduction zone magmatism. Blackwell Science, Cambridge, pp 100–105

Wyllie PJ (1982) Subduction products according to experimental prediction. Bull Geol Soc Am 93:468–476

Xie HS, Zhou WG, Zhu MX, Liu YG (2002) Elastic and electrical properties of serpentinite dehydration at high temperature and high pressure. J Phys-Condens Mat 14:11359–11363

Yang XZ (2012) Orientation-related electrical conductivity of hydrous olivine, clinopyroxene and plagioclase and implications for the structure of the lower continental crust and uppermost mantle. Earth Planet Sc Lett 317-318:241–250

Yang XZ, McCammon C (2012) Fe^{3+}-rich augite and high electrical conductivity in the deep lithosphere. Geology 40:131–134

Yang XZ, Keppler H, McCammon C, Ni HW, Xia QK, Fan QC (2011) Effect of water on the electrical conductivity of lower crustal clinopyroxene. J Geophys Res 116:B04208

Yang XZ, Keppler H, McCammon C, Ni HW (2012) Electrical conductivity of orthopyroxene and plagioclase in the lower crust. Contrib Mineral Petrol 163:33–48

Yoshino T, Laumonier M, Mcisaac E, Katsura T (2010) Electrical conductivity of basaltic and carbonatite melt-bearing peridotites at high pressures: implications for melt distribution and melt fraction in the upper mantle. Earth Planet Sc Lett 295:593–602

Zhang LT, Unsworth M, Jin S, Wei W, Ye GF, Jones AG, Jing JN, Dong H, Xie CL, Pape FL, Vozar J (2015) Structure of the central Altyn Tagh fault revealed by magnetotelluric data: new insights into the structure of the northern margin of the India-Asia collision. Earth Planet Sc Lett 415:67–79

Zhao ZF, Dai LQ, Zheng YF (2015) Two types of the crust-mantle interaction in continental subduction zones. Sci China Ser D 58:1269–1283

Zhu MX, Xie HS, Guo J, Zhang YM, Xu ZM (1999) Electrical conductivity measurement of serpentine at high temperature and pressure. Chin Sci Bull 44:1903–1907

Zhu MX, Xie HS, Guo J, Bai WM, Xu ZM (2001) Impedance spectroscopy analysis on electrical properties of serpentine at high pressure and high temperature. Sci China Ser D 44:336–345